Nonergodic metallic and insulating phases of Josephson junction chains

Manuel Pino[a], Lev B. Ioffe[a,b], and Boris L. Altshuler[c,1]

[a]Department of Physics and Astronomy, Rutgers, The State University of New Jersey, New Brunswick, NJ 08901; [b]Laboratoire de Physique Théorique et Hautes Energies, CNRS, UMR 7589, 75252 Paris Cedex 05, France; and [c]Physics Department, Columbia University, New York, NY 10027

Contributed by Boris L. Altshuler, November 20, 2015 (sent for review August 24, 2015; reviewed by Eugene Bogomolny and Leonid I. Glazman)

Strictly speaking, the laws of the conventional statistical physics, based on the equipartition postulate [Gibbs J W (1902) *Elementary Principles in Statistical Mechanics, developed with especial reference to the rational foundation of thermodynamics*] and ergodicity hypothesis [Boltzmann L (1964) *Lectures on Gas Theory*], apply only in the presence of a heat bath. Until recently this restriction was believed to be not important for real physical systems because a weak coupling to the bath was assumed to be sufficient. However, this belief was not examined seriously until recently when the progress in both quantum gases and solid-state coherent quantum devices allowed one to study the systems with dramatically reduced coupling to the bath. To describe such systems properly one should revisit the very foundations of statistical mechanics. We examine this general problem for the case of the Josephson junction chain that can be implemented in the laboratory and show that it displays a novel high-temperature nonergodic phase with finite resistance. With further increase of the temperature the system undergoes a transition to the fully localized state characterized by infinite resistance and exponentially long relaxation.

ergodicity | Josephson array | localization

The remarkable feature of the closed quantum systems is the appearance of many-body localization (MBL) (1): Under certain conditions the states of a many-body system are localized in the Hilbert space resembling the celebrated Anderson localization (2) of single particle states in a random potential. MBL implies that macroscopic states of an isolated system depend on the initial conditions (i.e., the time averaging does not result in equipartition distribution and the entropy never reaches its thermodynamic value). Variation of macroscopic parameters (e.g., temperature) can delocalize the many-body state. However, the delocalization does not imply the recovery of the equipartition. Such a nonergodic behavior in isolated physical systems is the subject of this paper.

We argue that regular Josephson junction arrays (JJAs) under the conditions that are feasible to implement and control experimentally demonstrate both MBL and nonergodic behavior. A great advantage of the Josephson circuits is the possibility to disentangle them from the environment, as was demonstrated by the quantum information devices (3). At low temperatures the conductivity σ of JJA is finite (below we call such behavior metallic), whereas as $T \to 0$ JJA becomes either a superconductor ($\sigma \to \infty$) or an insulator ($\sigma \to 0$) (4, 5). We predict that at a critical temperature $T = T_c$ JJA undergoes a true phase transition into an MBL insulator ($\sigma = 0$ for $T > T_c$). Remarkably, already in the metallic state JJA becomes nonergodic and cannot be properly described by conventional statistical mechanics.

In the bad metal regime the dynamical evolution starting from a particular initial state does not lead to the thermodynamic equilibrium, so that even extensive quantities such as entropy differ from their thermodynamic values. Starting with the seminal paper of Fermi et al. (6) the question of nonergodicity in nonintegrable systems was extensively studied (7). However, the difference between the long time asymptotics of the extensive quantities and their thermodynamic values was not analyzed to the best of our knowledge. We believe that the behavior of JJA that we describe here can be observed in a variety of nonlinear systems.

JJA is characterized by the set of phases $\{\phi_i\}$ and charges $\{q_i\}$ of the superconducting islands, ϕ_i and q_i for each i are canonically conjugated. The Hamiltonian H is the combination of the charging energies of the islands with the Josephson coupling energies. Assuming that the ground capacitance of the islands dominates their mutual capacitances (this assumption is not crucial for the qualitative conclusions) we can write H as

$$H = \sum_i \left[\frac{1}{2} E_C q_i^2 + E_J \left(1 - \cos(\phi_i - \phi_{i+1})\right) \right]. \qquad [1]$$

The ground state of the model Eq. **1** is determined by the ratio of the Josephson and charging energies, E_J/E_C, that controls the strength of quantum fluctuations: JJA is an insulator at $E_J/E_C < \eta$ and a superconductor at $E_J/E_C > \eta$ (4, 5) with $\eta \approx 0.63$ (*Supporting Information, section 1* and Fig. S1). The quantum transition at $E_J/E_C = \eta$ belongs to the Berezinsky–Kosterlitz–Thouless universality class (8). Away from the ground state in addition to E_J/E_C there appears dimensionless parameter U/E_J, where U is the energy per superconducting island ($U = T$ in the thermodynamic equilibrium at $T \ll E_J$).

The main qualitative finding of this paper is the appearance of a nonergodic and highly resistive "bad metal" phase at high temperatures, $T/E_J > 1$, which at $T \geq T_c \approx E_J^2/E_C$ undergoes the transition to the MBL insulator. In contrast to the $T = 0$ behavior, these results are robust (e.g., they are insensitive to the presence of static random charges). The full phase diagram in the variables E_J/E_C, T/E_J is shown in Fig. 1. We confirmed numerically that the bad metal persists in the classic ($E_J \gg E_C$)

Significance

Conventional equilibrium statistical physics that aims to describe dynamical systems with many degrees of freedom relies crucially on the equipartition postulate: After evolving for a sufficiently long time, the probabilities to find the system in states with the same energy are equal. Time averaging is thus assumed to be equivalent to the averaging over the energy shell—the famous ergodic hypothesis. In this study we show that this hypothesis is not correct for a large class of quantum many-body models that can be implemented in the laboratory. These models are predicted to show a novel type of behavior that we name bad metal, which is neither a many-body insulator nor a conventional conductor.

Author contributions: M.P., L.B.I., and B.L.A. performed research, analyzed data, and wrote the paper.

Reviewers: E.B., Université Paris-Sud, CNRS, Laboratoire de Physique Théorique et Modèles; and L.I.G., Yale University.

The authors declare no conflict of interest.

[1]To whom correspondence should be addressed. Email: bla@phys.columbia.edu.

This article contains supporting information online at www.pnas.org/lookup/suppl/doi:10.1073/pnas.1520033113/-/DCSupplemental.

limit although $T_c \to \infty$; it is characterized by the exponential growth of the resistance with T and violation of thermodynamic identities. We support these findings by semiquantitative theoretical arguments. Finally, we present the results of numerical diagonalization and tDMRG [time density matrix renormalization group (9)] of quantum systems that demonstrate both the nonergodic bad metal and the MBL insulator.

It is natural to compare the nonergodic state of JJA with a conventional glass characterized by infinitely many metastable states. The glass entropy does not vanish at $T=0$, that is, when heated from $T=0$ to the melting temperature the glass releases less entropy than the crystal [Kauzmann paradox (10)]. Similarly to glasses JJA demonstrates nonergodic behavior in both quantum and classical regimes. However, the ergodicity violation emerges as high rather than low temperatures transforming the Kauzmann paradox that arises at low temperatures into an apparent temperature divergence at high temperatures (discussed below).

Qualitative Arguments for MBL Transition

In a highly excited state $U \gg E_J$ the charging energy dominates: $E_C q^2 \sim U \gg E_J$. Accordingly, the value of the charge, $|q_i|$, and charge difference on neighboring sites, $\delta q_i = |q_i - q_{i+1}|$, are of the order of $q \sim \delta q \sim \sqrt{U/E_C}$. The energy cost of a unit charge transfer between two sites $\delta E \sim \sqrt{U E_c}$ exceeds the matrix element of the charge transfer, $E_J/2$, as long as $U \gg U_{MBL} = E_J^2/E_C$. According to refs. 1 and 2 the system is a nonergodic MBL insulator under this condition. Thus, we expect the transition to MBL phase at $T_c/E_J \propto E_J/E_C$ with the numerical prefactor close to unity, as follows from the computation presented in *Supporting Information, section 2* and Fig. S2. This computation also shows that resistivity is indeed infinite in this phase, contrary to the statement of work (11) that true MBL transition is impossible in translationally invariant systems.

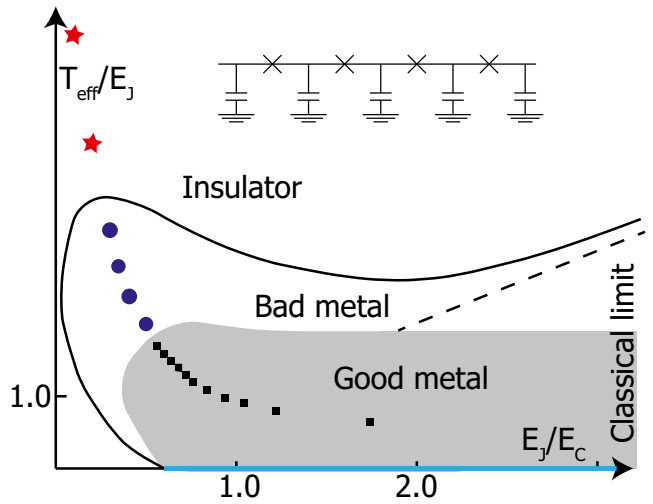

Fig. 1. Phase diagram of 1D Josephson junction array. The MBL phase transition separates the nonergodic bad metal with exponentially large but finite resistance from the insulator with infinite resistance. Cooling the nonergodic bad metal transforms it into a good ergodic metal. The points show approximate positions of the effective T/E_J for the quantum problem with a finite number of charging states. In bad metal as well as in insulator the temperature is ill-defined. So, T_{eff} should be understood as the measure of the total energy of the system. The red stars indicate insulator, blue circles bad metal, and squares good metal. The dashed line shows the estimate of MBL for large E_J/E_C discussed in the text. The superconductor is formed at $T=0$ at $E_J/E_C > 0.62$, as indicated by the thick blue line. This phase diagram is not sensitive to the presence of disorder for $T \gtrsim E_C$.

If $E_J/E_C \gg 1$ and $U \sim T \ll E_J$ the conductivity limited by thermally activated phase slips is exponentially large, $\sigma \sim \exp(E_J/T)$ (12, 13). As we show below, at $T \gg E_J$ in the metallic phase conductivity is exponentially small, $\sigma \sim \exp(-T/E_J)$, even far from the transition, $E_J \ll T \ll E_J^2/E_C$. The resistance in this state can exceed $R_Q = h/(2e)^2$ dramatically and still display the "metallic" temperature behavior ($dR/dT > 0$) (see Fig. 3).

Classical regime is realized at $E_C \to 0$ for fixed E_J and T. One can express the charge of an island q through the dimensionless time $\tau = \sqrt{E_J E_C}\, t$ as $q = \sqrt{E_J/E_C}\, d\phi/d\tau$. Because $q \sim \sqrt{T/E_C} \gg 1$, one can neglect the charge quantization and use the equations of motion

$$\frac{d^2\phi_i}{d\tau^2} = \sin(\phi_{i+1} - \phi_i) + \sin(\phi_{i-1} - \phi_i). \qquad [2]$$

Here $i = 1, \ldots, L$ and the boundary conditions are $\phi_0 = \phi_{L+1} = 0$. The ergodicity of this classic problem was discussed in ref. 14; however, the available time scales were too short to make convincing conclusions.

We solve Eq. **2** for the various initial conditions corresponding to a given total energy and compute the energy U_S contained in a part of the whole chain of the length $1 \ll l \ll L$ as a function of τ.

The ergodicity implies familiar thermodynamic identities; for example

$$\left(\langle U_S^2\rangle - \langle U_S\rangle^2\right) \Big/ T^2 = d\langle U_S\rangle/dT. \qquad [3]$$

This relation between the average energy of the subsystem, $\langle U_S\rangle$, and its second moment $\langle U_S^2\rangle$ turns out to be invalid for a bad metal. To demonstrate this we evaluated the average energy per site in this subsystem, $u = \overline{\langle U_S\rangle_\tau}/(E_J l)$, and the temporal fluctuations of this energy, $w_\tau = \overline{(\langle U_S^2\rangle_\tau - \langle U_S\rangle_\tau^2)}/(E_J^2 l)$. Here $\langle \ldots \rangle_\tau$ and the bar denote correspondingly averaging over the time and over the ensemble of the initial conditions. (Given the evolution time $\tau_{av}\langle \ldots \rangle_\tau$ averaging means averaging over the time interval τ_{ev} after initial evolution for time τ_{ev}.)

From Eq. **1** it follows that $u = T/(2E_J)$ at $T \gg E_J$ [$u(T)$-function is evaluated for arbitrary T/E_J in *Supporting Information, section 3*]. One can thus rewrite Eq. **3** as

$$w = \frac{T^2}{E_J}\frac{du}{dT} \approx 2u^2. \qquad [4]$$

Results of the numerical solution of Eq. **2** are compared with Eq. **3** in Fig. 2. For any given evolution time, τ_{ev}, the computed $w_\tau(u)$- dependence saturates instead of increasing as u^2 (Eq. **4**). At a fixed u, $w_\tau(u)$ increases with time extremely slowly. Below we argue that $w_\tau(u)$ does not reach its thermodynamic value even at $\tau \to \infty$. Violation of the thermodynamic identity implies that temperature is ill-defined, so the average energy u rather than T is the proper control parameter. The effective temperature, defined as $T_*(u) = E_J/\int_0^u du/w(u)$, is shown in Fig. 2, *Inset*.

Qualitative Interpretation

Large dispersion of charges on adjacent islands, $i, i+1$ at $u \gg 1$, implies quick change of the phase differences, $\phi_i - \phi_{i+1}$, with time. Typical current between the two neighbors $E_J \sin(\phi_i - \phi_{i+1})$ time-averages almost to zero. However, accidentally the frequencies, $\omega_i = d\phi_i/dt$, get close. In the classical limit the difference $\omega_i - \omega_{i+1}$ can be arbitrary small. Such pair of islands is characterized by one periodic in time phase difference. Contrarily, three consecutive islands with close frequencies $|\omega_i - \omega_{i+1}| \sim |\omega_i - \omega_{i-1}| \lesssim 1$ experience chaotic dynamics that contains arbitrary small frequencies, similarly to work (15). For uncorrelated frequencies with variances $u \gg 1$, a triad of

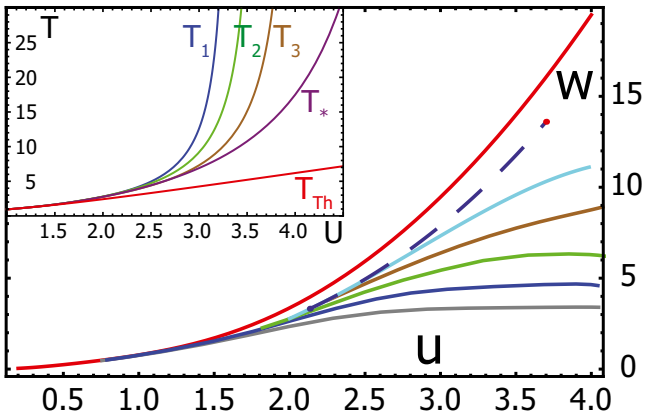

Fig. 2. Energy fluctuations as a function of average energy per island for different evolution times ($\tau_{ev} = 1, 2, 4, 8, 16 \times 10^4$) in a small subsystem ($L_{sub} = 0.1 - 0.2L$) located in the center of the system; the dashed line is the extrapolation to infinite times as explained in the text. A single point (red) obtained by direct computations up to $\tau_{ev} = 210^6$ at which timescales the time dependence practically disappears for $L \lesssim 100$. The upper (red) curve corresponds to the thermodynamic identity Eq. **3**. (*Inset*) The effective temperature defined by the energy fluctuations determined at different timescales: $\tau_{ev} = 2,4,8 \times 10^4$ ($T_1 - T_3$, respectively) and by their extrapolation to infinite times (T_*), their comparison with the temperature expected in thermodynamic equilibrium, T_{Th}.

islands $(i-1, i, i+1)$ is chaotic with the probability $1/u \ll 1$, that is, such triads are separated by large quiet regions of a typical size $r_t \sim u \gg 1$. The low-frequency noise generated by a chaotic triad decreases exponentially deep inside a quiet region. Provided that $\omega \ll \omega_{i+m}$, $m = 0 \ldots r$ the superconducting order parameter $z_i(\omega) = \int d\tau \exp(i\phi_i + i\omega\tau)$ at site i satisfies the recursion relation

$$z_{i+r}(\omega) = z_i(\omega) \prod_{m=0}^{r-1} \frac{1}{2\omega_{i+m}^2}, \qquad [5]$$

which implies the log-normal distribution for the resistances $R_{j,j+r}$ of quiet regions (*Supporting Information, section 4*):

$$\left\langle \ln^2(R/R_t) \right\rangle = \ln R_t \qquad [6]$$

$$\ln R_t = \langle \ln R \rangle = u \ln(u), \qquad [7]$$

where R_t is the typical resistance of a quiet region. The resistance of the whole array is the sum of the resistances of the quiet regions. The mean number of these regions in the chain equals to $N = L/r_t \gg 1$, its fluctuations being negligible. For the log-normal distribution the average resistance of a quiet region, $\langle R \rangle$, is given by $\langle R \rangle = R_t^{3/2}$. For the resistivity, ρ, we thus have $\rho = N\langle R \rangle / L = R_t^{3/2}/r_t$. According to Eq. **7**

$$\ln \rho r_t \approx \frac{3}{2}(\gamma + \ln u) r_t \approx u(\ln u + \gamma), \qquad [8]$$

where $\gamma = 0.577$ is Euler constant.

To determine the current caused by voltage V across the chain we solved Eq. **2** with modified boundary conditions, $\phi_0 = 0$, $\phi_{L+1} = Vt$. The results confirm the prediction Eq. **8** (Fig. 3). The range of the resistances set by realistic computation time is too small to detect the logarithmic factor in Eqs. **7** and **8**; however, a relatively large slope, $d \ln \rho / du \approx 3.0$, at $u = 3.5$ is consistent with Eq. **8** that gives $d\ln\rho/du \approx 2.5 + 1.5 \ln u - 1/u$.

The qualitative picture of triads separated by log-normally distributed resistances of silent regions allows one to understand the long time relaxation of $w_\tau(u)$ in the subsystem of length l (Fig. 2). Each resistance can be viewed as a barrier with a tunneling rate $\sim 1/R$. For a given time τ the barriers with $\tau \ll R$ can be considered impenetrable, whereas the barriers with $\tau \gg R$ can be neglected. As a result, the barriers with $R \geq \tau$ break the system into essentially independent quasiequilibrium regions (QER) of the typical size

$$l_\tau \sim \frac{r_t}{\sqrt{2\pi \ln R_t}} \exp\left[\frac{\ln^2(\tau/R_t)}{2 \ln R_t}\right]. \qquad [9]$$

If $l \gg r_t$ and $\tau \lesssim \exp[\sqrt{\ln(l/r_t) \ln R_\tau}]$ the subsystem contains $l_\tau/l \gg 1$ QER, so that $w \propto l_\tau/l$. At longer times, $l_\tau \gg l$, the subsystem is in equilibrium with a particular QER and $w \propto l/l_\tau$. The full dependence on time can be interpolated as

$$w_\tau = \frac{w_\infty}{1 + \beta \exp(-\alpha \ln^2(\tau/\tau_0))}, \qquad [10]$$

where $\alpha = (2 \ln R_t)^{-1}$, $\beta = \sqrt{\pi/\alpha}(l/r_t)$ and $\tau_0 = R_t$.

The numerical simulations confirm that the energy variance w relaxes in agreement with Eq. **10** as shown in Fig. 4. The best fit to Eq. **10** yields parameters close to the expected, $\ln R_t = \ln \rho(u) r_t$, $r_t \approx u$. Extrapolation to inifinite times and sizes gives $w_\infty(\infty) \approx 10.0$ of $w_\infty(l)$ to large l, which is significantly smaller than thermodynamic value $w_{Th} = 14.0$ at $u = 3.5$.

Another test of the ergodicity follows from the fluctuation-dissipation theorem (FDT) that relates conductivity and current fluctuations. In the low frequency limit the noise power spectrum is $S(\omega \to 0) = 2T_{eff}/R$, where T_{eff} is the effective temperature (Fig. 5), which we extracted from the numerical data. We found that $T_{eff} > T_{Th}$ for $u \gtrsim 1$, where T_{Th} is thermodynamic temperature. In particular, $T_{eff} \approx 1.6 T_{Th}$ for $u = 3.5$, which is close to $T_*(u)$ shown in Fig. 2, *Inset*. Note that both the energy and current fluctuations are less than expected in equilibrium.

Quantum Behavior

In contrast to a classical limit $E_C \to 0$ in the quantum regime $E_C > 0$ we expect at $T = T_c$ a MBL phase transition between two nonergodic states: the insulator ($\rho = \infty$) and a bad metal ($\rho < \infty$). For $E_J \gg E_C$ the bad metal can be described classically at $T \ll T_c \sim E_J^2/E_C$. Our previous discussion suggests that the bad metal is nonergodic in a broad range of the parameters, T/E_J and E_J/E_C. To verify this conjecture numerically we reduced the

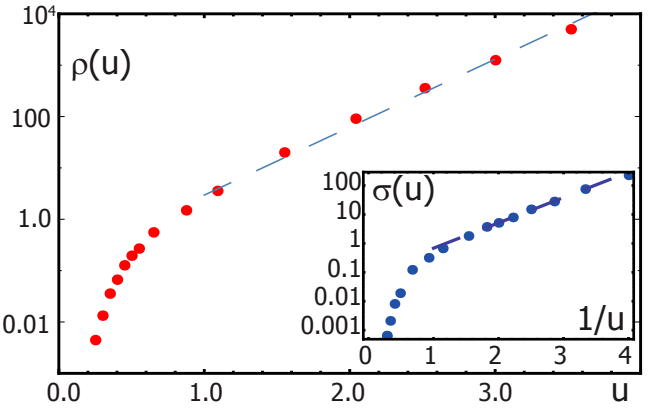

Fig. 3. Resistivity as a function of the internal energy. At high energies resistivity is exponentially large due to large regions of almost frozen charges (discussed in the text). (*Inset*) At low energies (temperatures) exponentially large conductivity is limited by exponentially rare phase slips. High u points require computation times $\tau_{ev} \sim 10^8$.

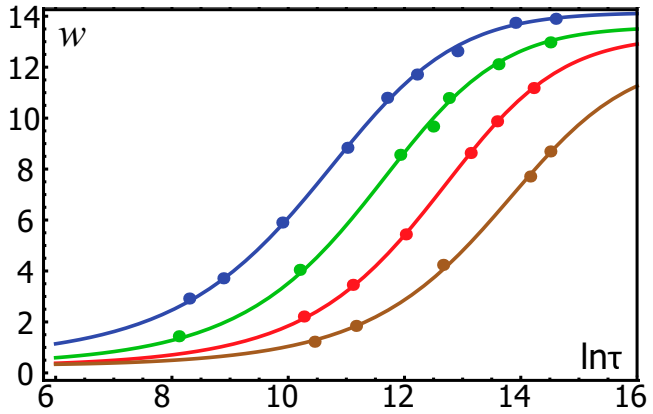

Fig. 4. Time dependence of energy fluctuations for the subsystems of different sizes $l = 10, 20, 40, 80$ (left to right) and their fits to log-normal law Eq. **10**. The length of the full system was $L = 5l$. The best fit shown here corresponds to the value $\alpha = 0.05$, $\beta/l = 1.0 - 1.5$ and $\ln \tau_0 \approx 3.0 - 4.5$. The values for larger sizes ($\beta/l \approx 1$ and $\ln \tau_0 \approx 4.5$) agree very well with the ones expected for R_t obtained in the computation of the resistance at $u = 3.5 : \ln R_t \approx 5.0$. This yields $r_t \approx 5.0$, $\beta/l \approx 1.1$ and $\ln \tau_0 \approx 5.0$.

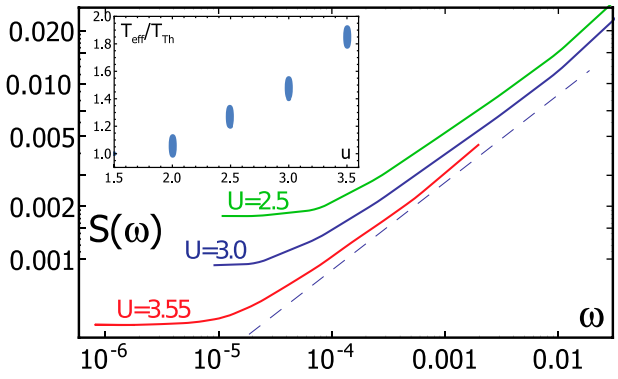

Fig. 5. Spectrum of current noise fluctuations, $S(\omega)$ for different internal energies, $U = 2.5, 3.0, 3.55$. The dashed line shows $S(\omega) \sim \omega^{1/2}$ dependence. (*Inset*) The effective temperature determined from FDT relation.

Hilbert space of the model Eq. **1** to a finite number of charging states at each site, $q_i = 0, \pm 1, \pm 2$ (RHS model). We analyzed the time evolution of entanglement entropy, $S\{\Psi\}$, of the left half of the system. The entropy was averaged over the initial states from the ensemble of product states in the charge basis, $S_t(L) \equiv \langle S\{\Psi\}\rangle_{\Psi_{in}}$ that correspond to zero total charge. As a result, we obtained the Gibbs entropy at $T = \infty$ [all states have the same weight $\exp(-H/T) \equiv 1$].

Fig. 6, *Inset* shows the time dependence of the entropy at $E_J/E_C = 0.3$ that corresponds to the bad metal regime (discussed below). A slow saturation of the entropy follows its quick initial increase. It is crucial that the saturation constant, $S_\infty(L)$, is significantly less than its maximal value, $S_{Th}(L) = L \ln 5$ expected at $T = \infty$ equilibrium. Furthermore, $dS_\infty(L)/dL < \ln 5$, indicating that $S_\infty - S_{Th}$ is extensive and the system is essentially nonergodic.

Fig. 6 presents S_∞ as a function of E_J/E_C. Note that S_∞ is measurably less than S_{Th} for $E_J/E_C < 0.6 - 1$. For $E_J/E_C \gg 1$, the entropy saturation is quick, and the accuracy of the simulations does not allow us to distinguish S_∞ from S_{Th} (see Figs. S3 and S4). We thus are unable to conclude whether the system is truly ergodic or weakly nonergodic at $E_J/E_C \gg 1$. The former behavior would imply a genuine phase transition between bad and good metals, whereas the latter corresponds to a cross-over.

Deep in the insulator the time dependence of the entropy is extremely slow, roughly linear in $\ln t$ in a wide time interval (*Supporting Information, section 5*). This resembles the results of the works (16, 17) for the conventional disordered insulators. The extremely long relaxation times can be attributed to rare pairs of almost degenerate states localized within different halves of the system. The exponential decay with distance of the tunneling amplitude that entangles them leads to the exponentially slow relaxation.

To locate the MBL transition we analyzed the time dependence of the charge fluctuations. In a metal the charge fluctuations relaxation rate depends weakly (as a power law) on the sample size, in contrast to the exponential dependence in the insulator. Comparing the dependencies of the rates on the system size for different E_J/E_C (Fig. 7) we see that the transition happens in the interval $0.05 < E_J/E_C < 0.3$.

The variances of the charge in the RHS model at $T = \infty$ and in the problem Eq. **1** at finite T coincide at $T = 2E_C$. Thus, we expect that the results of the quantum simulations describe the behavior of the model Eq. **1** at $T/E_J \sim E_C/E_J$ yielding the hyperbola shown in Fig. 1. The MBL transition at $E_J/E_C \sim 0.2$ in $T = \infty$ RHS model corresponds to the transition temperature $T_c \sim 10E_J$ in model Eq. **1**. The transition line shown in Fig. 1 is a natural connection of this point with $T_c \approx E_J^2/E_C$ asymptotic at $E_J/E_C \gg 1$, discussed above. The maximum of the transition temperature is natural. Indeed, at $E_J < E_C$ the charge fluctuates weakly at low T, in the opposite limit $E_J < E_C$ the phase is well-defined, whereas at $E_J \sim E_C$ the quantum fluctuations are largest.

Possible Experimental Realization

MBL and the violation of the ergodicity can be observed only at sufficiently low temperatures when one can neglect the effects of thermally excited quasiparticles that form the environment to model Eq. **1**. This limits temperatures to $T \lesssim 0.1\Delta$, where Δ is the superconducting gap. To explore the phase diagram one has to vary both T/E_J and E_J/E_C in the intervals $1 \lesssim T/E_J \lesssim 5$ and $0.1 \lesssim E_J/E_C \lesssim 5$. The former condition can be satisfied if each junction is implemented as a superconducting quantum interference device loop with individual Josephson energy $E_J^{(0)} \sim T_{max} = 0.1\Delta$ so that $E_J = 2\cos(e\Phi/\pi\hbar)E_J$, where Φ is flux through the loop. The latter condition requires enhancing ground capacitance of each island, which should exceed the capacitance of the junctions in order for the model Eq. **1** to be relevant. Realistic measurements of such array include

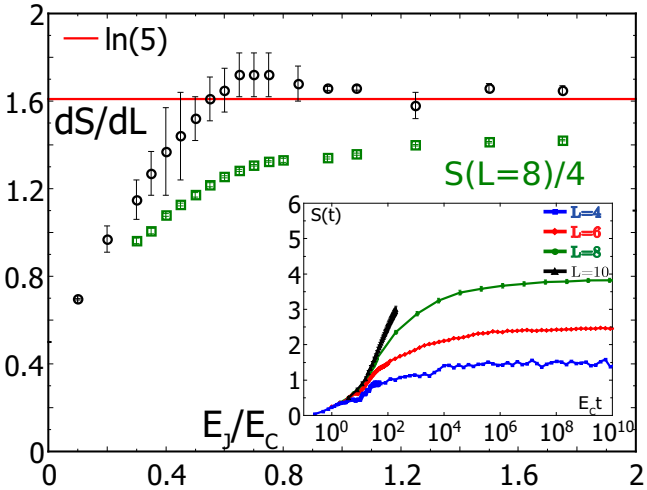

Fig. 6. Entropy per spin in thermodynamic limit extrapolated to $t = \infty$. (*Inset*) $S(t)$ dependence in the bad metal regime at $E_J/E_C = 0.3$ that shows slow relaxation of the entropy to its saturation value.

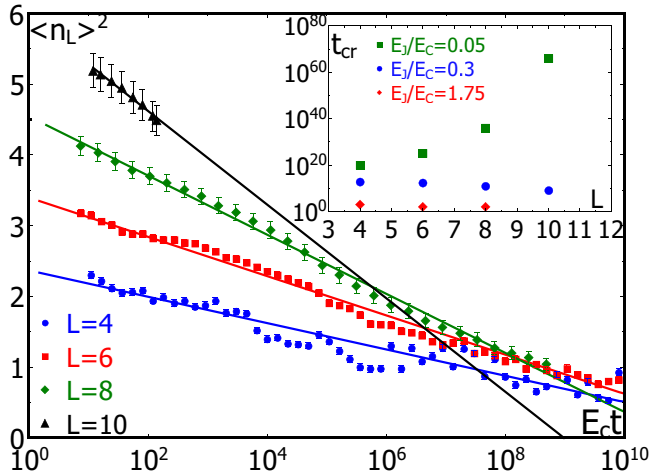

Fig. 7. Charge relaxation in a bad metal ($E_J/E_C = 0.3$). The characteristic timescale, t_{cr}, can be defined by the extrapolated crossing point of $\langle n^2 \rangle$ with the t axis. The crossing point t_{cr} shows dramatically different behavior for the insulator and metal (*Inset*): In the good metal this time is very short, and in the bad metal it is dramatically longer but does not increase with size whereas in the insulator it is extremely long and grows with size.

resistance $R(T, E_J)$ and current noise. Here we predict a fast growth with temperature and divergence at T_c of the resistivity and violation of FDT.

Recently numerical studies (18–20) investigated whether MBL can exist in disorder-free 1D systems. These works studied models different from ours. De Roeck and Huveneers (21) argued that the localization should happen in a similar model at infinite T. Very recently the same group (11) claimed to prove the absence of true localization in periodic systems. This proof was based on the assumption of ergodicity, specifically the eigenstate thermalization hypothesis, in the metallic regime. This assumption (which allowed the authors to argue in terms of moving ergodic bubbles) is incorrect for the model studied here because the metallic phase is generally nonergodic. Furthermore, results concerning Kullback–Liebler (KL) divergence (Fig. S5 and *Supporting Information, section 6*) indicate that the metallic phase is not fully described by Gaussian ensemble at any value of parameters. Qualitatively, a bubble is subject to the effective random potential, which originates from its boundaries and is exponentially stronger than the bubble bandwidth, resulting in the bubble localization. Similarly one can ask why Arnold diffusion does not lead to delocalization in the classical limit (22). The reason is the random environment created by the triad neighbors that destroys subtle many-body resonance. We have checked numerically that a short classical chain does not display triad diffusion.

In conclusion, we presented strong numerical evidence for the MBL transition and its semiquantitative description in a regular, disorder-free Josephson chain. Probably the most exciting finding is the intermediate nonergodic conducting phase (bad metal) between the MBL insulator and good ergodic metal. This phase distinguishes Josephson junction chain from the spin1/2 Heisenberg 1D model in a random field (23–25), where the ergodicity is believed to be violated only in the MBL regime (25). The ergodicity violation in a wide range of parameters is in contrast to the one-particle Anderson localization in a finite-dimensional space where the nonergodic behavior is limited to the critical point. However, the signatures of the "non-Gibbs regime" in the discrete nonlinear Schrodinger equation (26, 27), the appearance of the nonergodic states in a single-particle problem on the Bethe lattice, as well as the dominance of single-path relaxation close to the critical point of superconductor–insulator transitions on the Bethe lattice (28, 29) make us believe that the intermediate nonergodic phase is a generic property of MBL transition rather than an exception. Further work is needed to establish the domain of the applicability of these results as well as the nature of the transition between bad and good metals.

Methods

Simulation of the JJA in the Classical Regime. At large u averaging out temporal fluctuations requires exponentially long times. Moreover, at $u \gg 1$ the resistance increases with u factorially, leading to a strong heating in the computation of resistance unless the measurement current is factorially small. Observation of a small current against the background of a low-frequency noise requires increasingly long times. Accordingly, for the realistic evolution times $\tau_{ev} \lesssim 10^8$ the resistance can be computed only for $u < 4.0$.

Simulation of the Quantum Problem. The time dependence of the entropy and the charge fluctuations for system of sizes $L = 4,6,8$ was computed using exact diagonalization in a symmetric subspace under charge conjugation. The tDMRG method was used for larger sizes but accuracy limits the range of times that we could study. In all simulations we impose the particle number conservation and open boundary conditions.

ACKNOWLEDGMENTS. We thank I. L. Aleiner, M. Feigelman, S. Flach, V. E. Kravtsov, and A. M. Polyakov for useful discussions. This work was supported in part by Templeton Foundation Grant 40381, Army Research Office Grant W911NF-13-1-0431, and Agence Nationale de la Recherche QuDec.

1. Basko DM, Aleiner IL, Altshuler BL (2006) Metal-insulator transition in a weakly interacting many-electron system with localized single-particle states. *Ann Phys* 321(5):1126–1205.
2. Anderson PW (1958) Absence of diffusion in certain random lattices. *Phys Rev* 109(5): 1492–1505.
3. Devoret MH, Schoelkopf RJ (2013) Superconducting circuits for quantum information: An outlook. *Science* 339(6124):1169–1174.
4. Efetov KB (1980) Phase transitions in granulated superconductors. *Zh Eksp Teor Fiz Pis'ma Red* 78(5):2017–2032.
5. Fazio R, van der Zant H (2001) Quantum phase transitions and vortex dynamics in superconducting networks. *Phys Rep* 355(4):235–334.
6. Fermi E, Pasta J, Ulam S (1955) Studies of the Nonlinear Problems. I. Los Alamos Report LA-1940 (Los Alamos Scientific Lab, Los Alamos, NM).
7. Galavotti G (2008) *The Fermi–Pasta–Ulam Problem* (Springer, Berlin).
8. Kosterlitz JM, Thouless DJ (2013) *40 Years of Berenzinskii-Kosterlitz-Thouless Theory* (World Scientific, Singapore), pp 1–67.
9. White SR (1992) Density matrix formulation for quantum renormalization groups. *Phys Rev Lett* 69(19):2863–2866.
10. Kauzmann W (1948) The nature of the glassy state and the behavior of liquids at low temperatures. *Chem Rev* 42:219–256.
11. De Roeck W, Huveneers F (2014) Scenario for delocalization in translation-invariant systems. *Phys Rev B* 90:165137.
12. Tinkham M (1996) *Introduction to Superconductivity* (McGraw-Hill, New York).
13. Schmidt VV (2002) *The Physics of Superconductors: Introduction to Fundamentals and Applications* (Springer, Berlin).
14. Escande D, Kantz H, Livi R, Ruffo S (1994) Self-consistent check of the validity of Gibbs calculus using dynamical variables. *J Stat Phys* 76(1):605–626.
15. Chirikov BV (1979) A universal instability of many-dimensional oscillator systems. *Phys Rep* 52(5):265–379.
16. Bardarson JH, Pollmann F, Moore JE (2012) Unbounded growth of entanglement in models of many-body localization. *Phys Rev Lett* 109(1):017202.
17. Serbyn M, Papić Z, Abanin DA (2013) Universal slow growth of entanglement in interacting strongly disordered systems. *Phys Rev Lett* 110(26):260601.
18. Yao NY, Laumann CR, Cirac JI, Lukin MD, Moore JE Quasi many-body localization in translation invariant systems. arXiv:1410.7407, 2014.
19. Schiulaz M, Silva A, Müller M (2015) Dynamics in many-body localized quantum systems without disorder. *Phys Rev B* 91:184202.
20. Papic Z, Stoudenmire EM, Abanin DA (2015) Is many-body localization possible in the absence of disorder? arXiv:1501.00477.
21. De Roeck W, Huveneers F (2014) Asymptotic quantum many-body localization from thermal disorder. *Commun Math Phys* 332(3):1017–1082.
22. Basko DM (2011) Weak chaos in the disordered nonlinear schrdinger chain: Destruction of Anderson localization by Arnold diffusion. *Ann Phys* 326(7):1577–165.
23. Oganesyan V, Huse DA (2007) Localization of interacting fermions at high temperature. *Phys Rev B* 75(15):155111.
24. Oganesyan V, Pal A, Huse DA (2009) Energy transport in disordered classical spin chains. *Phys Rev B* 80(11):115104.
25. Luitz DJ, Laflorencie N, Alet F (2015) Many-body localization edge in the random-field heisenberg chain. *Phys Rev B* 91:081103.

26. Rasmussen KO, Cretegny T, Kevrekidis PG, Gronbech-Jensen N (2000) Statistical mechanics of a discrete nonlinear system. *Phys Rev Lett* 84(17):3740–3743.
27. Flach S, Gorbach AV (2008) Discrete breathers – Advances in theory and applications. *Phys Rep* 467(1–3):1–116.
28. Feigel'man MV, Ioffe LB, Mezard M (2010) Superconductor-insulator transition and energy localization. *Phys Rev B* 82(18):184534.
29. Cuevas E, Feigel'man M, Ioffe L, Mezard M (2012) Level statistics of disordered spin-1/2 systems and materials with localized Cooper pairs. *Nat Commun* 3:1128.
30. Buonsante P, Vezzani A (2007) Ground-state fidelity and bipartite entanglement in the Bose-Hubbard model. *Phys Rev Lett* 98(11):110601.
31. Pino M, Prior J, Somoza AM, Jaksch D, Clark SR (2012) Reentrance and entanglement in the one-dimensional bose-hubbard model. *Phys Rev A* 86:023631.